JNPS 5 (1), 74-84 (2019)
ISSN: 2392-473X

Research Article

AN INFRARED SURVEY OF ISOLATED NEBULAR STRUCTURES AT GALACTIC LATITUDES 16.98˚& 1.98˚ IN IRAS MAP

A. S. Thapa[1,2,*], M. S. Paudel[3], B. Pant[1]
[1]*St. Xavier's College, Maitighar*
[2]*Nepalese Center for Research in Physical Sciences*
[3]*Tri-Chandra Multiple Campus, Tribhuvan University*
[*]***Corresponding Email:*** *aditya.thapa@ncrps.org.np*

ABSTRACT

Two isolated far infrared dust structures (~2.61pc × 1.57pc and ~82.99pc × 39.99pc) at galactic coordinates: (353.01˚, 16.98˚) and (18.42˚, 1.98˚), were selected. We adopted the distance of the first structure to be about 139 pc and that of the second structure to be 2.6 kpc. In this present work we have studied the flux density variation and calculated dust color temperature and mass profile of the dust and Jeans mass of the structures using the data reduction software ALADIN v9. Our aim was to test whether this region is star forming or not. We also calculated the size and inclination angle of our structures. The dust color temperature is found to lie in the range 20.75 K to 35.90 K for the first region and 22.52 K to 45.63 K for the second region. The total mass of gas for the first structure is found to be about 20.99 $M_\odot$ and Jeans mass is found to be 180.9 $M_\odot$, which is significantly greater than the total mass of the structure, suggesting no possibility of star formation activity for the first region. For the second region, the total mass of gas and the Jeans mass are found to be 5621.61 $M_\odot$ and 6005.04 $M_\odot$ respectively. The mass of the region is still significantly lesser than the Jeans mass. Thus, we conclude that this region is also probably not a star forming region. Also the study of inclination angle suggests that the three-dimensional shape of structures is non uniform and regularly shaped.

Keywords: Infrared astronomy, IRAS, dust mass, temperature, dust geometry, star-formation, Inclination angle, Nebulae.

INTRODUCTION

Dust present in galaxies absorbs starlight from around it and this absorbed energy is then reradiated at infrared (IR) and far-IR (FIR) wave lengths by the interstellar dust [1]. It is a significant constituent of the Galaxy. It blocks almost all but relatively close regions at visual and ultraviolet frequencies and then the reradiating of this absorbed energy in the far-infrared wavelengths comprise of about 30% of the Galaxy's total luminosity [2]. Dust grains play an essential part in the astrophysics of the interstellar medium, from the thermodynamics and chemistry of the gas, to the dynamics of star formation [3]. The far-infrared emission from interstellar dust eliminates the gravitational collapse of clouds, permitting star formation to take place [2].

The Infrared Astronomical Satellite (IRAS) made an all-sky survey at 12, 25, 60, and 100 μm band of infrared radiation with a cryogenically cooled telescope orbiting above the Earth's atmosphere. It has been seen that the infrared observations over the last few decades have been increasingly important in understanding the objects of the solar system and regions of star formation, in identifying galaxies with large bursts of newly formed stars, in seeing through astronomical sources concealed by interstellar dust, and in explaining the emission mechanisms present in active galactic nuclei [4].

In this paper, we investigate isolated dust structures in IRAS maps by performing a systematic search in all wavelength band of the IRAS survey. We study various properties of two isolated nebular structures such as; flux density for infrared radiation, dust color temperature and mass distribution. We

subsequently, look whether the structures are star forming or not. We also study the three dimensional features of the structure by studying he inclination angles of various layers of the structure.

DATA

Systematic Search in the IRAS Map

We used Sky view Virtual Observatory (http://skyview.gsfc.nasa.gov) in order to search for an isolated nebular structure for different wavelength IRAS bands. We carried a systematic search of IRAS maps available in the Sky view Virtual Observatory. First, we inspected our region in 4˚×4˚sized images through the entire range of longitude for particular galactic latitudes. We conducted such searches for four different galactic latitudes (-20˚, 2˚, 16˚, and 20˚).

We then selected a proper centers for our selected structures which were (353.01˚, 16.98˚) and (18.42˚, 1.98˚) in Galactic coordinates and also we narrowed down our region of interest into a 2˚×2˚image for more specific study of the selected isolated structures. These final set of images that we finalized for our study are as follows:

Region-I (353.01˚, 16.98˚)

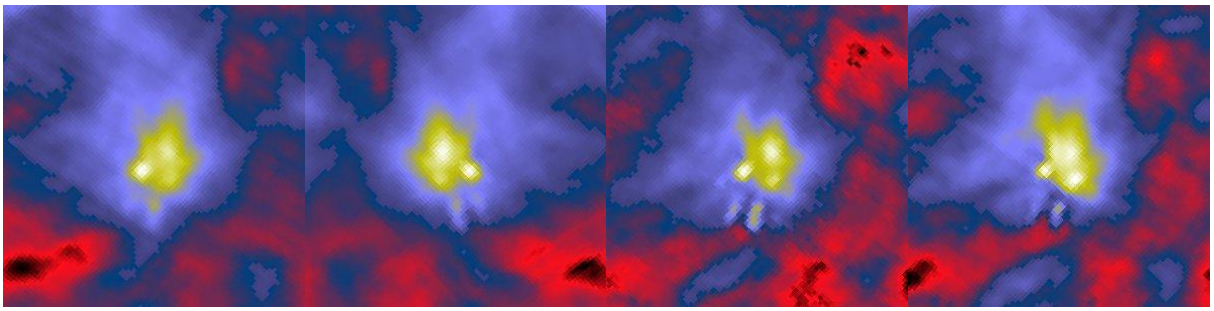

Fig. 1: *Selected 2˚×2˚IRAS images (100 μm, 60 μm, 25 μm and 12 μm) at Galactic coordinate (353.01˚, 16.98˚).*

Region-II (18.42˚, 1.98˚)

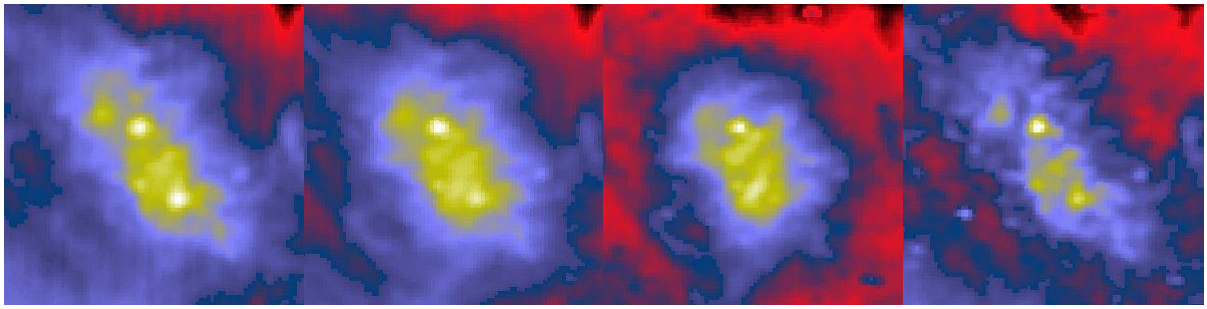

Fig. 2: *Selected 2˚×2˚IRAS images (100μm, 60μm, 25μm and 12μm) at Galactic coordinates (18.42˚, 1.98˚).*

Also SIMBAD (http://simbad.u-strasbg.fr) was used to find the degree of study made on the nebular structure and to identify the structures around it. We found that structure found in Galactic longitude 353.01˚and Galactic latitude 16.98˚(Region-I) was an isolated structure in the famous star forming region ρ-Ophiuchus Molecular Cloud (Lynds 1688) [5, 6]. We found that the structure in Galactic longitude 18.42˚and Galactic latitude 1.98˚ (Region-II) was less studied and hence also making it appropriate for our study.

METHODOLOGY

Data Reduction and Background Correction

Each pixel of the FITS image of our region of interest was analyzed using the software ALADIN v9. There are various source of energy around our region of interest, which can be known from SIMBAD (http://simbad.u-strasbg.fr), can increase the flux of region of interest. The flux emitted by other sources lying nearby the region of interest but not from the region of interest is called background flux. The flux density obtained from ALADIN is total flux density (background flux +flux due to

dust). Flux density obtained is corrected by subtracted it with the background flux density. The average value of the background flux is obtained by noting and summing of the flux densities of the minima around the region of interest and averaging them. When this background flux is subtracted from the obtained flux density of each pixel in the region of interest, it is said to be background corrected flux density. The flux density throughout this work including the all the graphs and the tables represents the background corrected flux density.

Contours and Diameters

With the help of software ALADIN v9, we have drawn contour maps to distinguish the regions with maximum flux in the region of interest. Fig shows a contour map at 24 and 146 contour levels for Region-I and at 24, 77, 100 and 131 contour levels for Region-II.

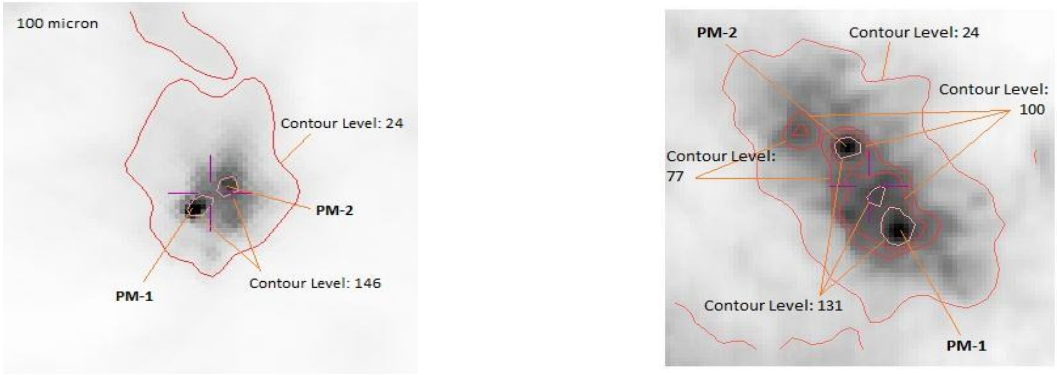

Fig. 3: *2˚×2˚IRAS 100 μm FITS image centered at Galactic longitude: 353.01˚, Galactic latitude: 16.98˚(Region-I) and Galactic longitude: 18.42˚, Galactic latitude: 1.89˚.*

Two maxima can be seen. They are represented by PM1 and PM2. The contour level is fixed between 24 and 146 (in relative units) for Region-I and between 24 and131 (in relative units) for Region-II. The two maxima in the region of interest at the following position:

For Region-I: PM1 is at RA (J2000) = $16^h26^m29.30^s$, Dec. (J2000) = −24˚23’05.2″ and PM2 is at RA (J2000) = $16^h25^m39.01^s$, Dec (J2000) = −24˚26′ 59.03″.

For Region-II: PM1 is at RA (J2000) = $18^h16^m45.29^s$, Dec. (J2000) = −12˚12’34.5″ and PM2 is at RA (J2000) = $18^h17^m52.79^s$, Dec (J2000) = −11˚44′ 04.77″.

We obtained the largest and smallest diameters for the regions, i.e. major axis and minor axis, by drawing lines passing through the maximum flux region, PM1. The figure below shows the major axis, minor axes.

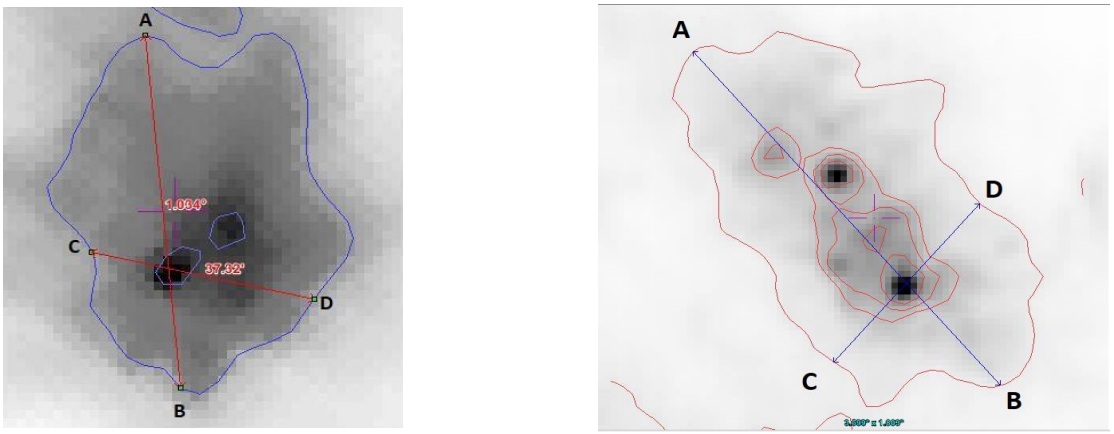

Fig. 4: *Figure showing major axis (AB), minor axis (CD) and line joining themaximum flux region, while studying the flux variation in the field of view of 100 μm FITS image of Region-I (left) and Region-II (right).*

Dust Temperature Estimation

The corrected flux density at each pixel inside the region of each of the maxima is calculated from the IRAS 100μm image. Similarly the corresponding flux densities are calculated from the IRAS 60μm image. Using the ratio of the flux density in the IRAS 60μm to the flux density in the IRAS 100μm in expression (1) given below, dust color temperature is calculated.

$$T_d = \frac{-96}{ln\{R \times 0.6^{(3+\beta)}\}} \ldots\ldots\ldots\ldots\ldots\ldots (1)$$

Where R is given by,

$$R = \frac{F(100\mu m)}{F(60\mu m)} \ldots\ldots\ldots\ldots\ldots\ldots\ldots (2)$$

Where$F(100\mu m)$ and$F(60\mu m)$ are the flux density at 100μm and 60μm.

Dust Mass Estimation

Dust masses are estimated from the infrared background corrected flux densities at100μm image, following the analysis of Schnee *et. al.*[13] The infrared flux can be measured from IRAS Sky View images using ALADIN v9.The resulting dust mass depends on the physical and chemical properties of the dust grains, the adopted dust temperature and the distance to the object. The final expression for the dust mass can be written as:

$$M_{dust} = \frac{4}{3}\frac{a\rho}{Q_v}\frac{S_v D^2}{B(v,T)} \ldots\ldots\ldots\ldots\ldots\ldots\ldots (3)$$

Where, a= weighted grain size; ρ= grain density; Q_v= grain emissivity; S_v= f×MJy/Str×5.288×10^{-9} where, 1 MJy/Str = 1×10^{-20}kgs^{-2}and f = relative flux density measured from the image (IRAS 100 μm image); D = distance of the structure $B(v,T)$ = Planck's function, which is the function of the temperature and the frequency and given by the expression:

$$B(v,T) = \frac{2hv^3}{c^2}\left[\frac{1}{exp\left(\frac{hv}{KT}-1\right)}\right] \ldots\ldots\ldots\ldots (4)$$

Where, h= Planck's constant; c= speed of light; ν = frequency at which the emission is observed; T = the average temperature of the region. Value of various parameters we use in the calculation of the dust mass in our region of interest are as follows: a= 0.1μm; ρ= 3000 kgm^{-3}; Q_v= 0.0010 for 100 μm and 0.0046 for 60μm respectively [12]. Using these values the expression (3) takes the form:

$$M_{dust} = 0.4\left[\frac{S_v D^2}{B(v,T)}\right] \ldots\ldots\ldots\ldots\ldots\ldots\ldots (5)$$

Inclination Angle

The inclination angle (i) is the angle between the line of sight and the normal vector of the plane of the structure. This can be estimated by using the following formula [10],

$$cos^2 i = \frac{\left(\frac{b}{a}\right)^2 - q^{*2}}{1 - q^{*2}} \ldots\ldots\ldots\ldots\ldots\ldots\ldots (6)$$

Where, (b/a) is the ratio of minor to major diameter and q* is the intrinsic flatness of the structure. The intrinsic flatness is closely related to nebula morphology. It depends on the amount of molecular hydrogen and the dust. The grain in the dust gains energy from the photoelectric heating and the low energy cosmic rays heating. Due to this vibrational degree of freedom is greatly enhanced. This makes the cloud to be flat (opening angle gradually increase with the dilution and vibrational excitation of the dust). Thus the range of the intrinsic flatness of the cloud is wide. We varied the intrinsic flatness from 0.13 to 0.33 for the molecular cloud such that it covers a wide spectrum of possible outcomes. around the value 0.20 used for a morphologically unknown structure [7].

RESULTS AND DISCUSSION

Flux densities

The background corrected flux densities are seen to be concentrated more towards the central region of both structure in 100μm as well as 60μm images. A few peculiarities have been observed nevertheless. For the first region, there are two peaks of 60 μm band which is not seen in the 100 μm band for the same region. This might suggest the chemistry of the isolated nebula. Similarly, only a single bump is seen in the 60 μm band for the second region, whereas there are two bumps in emission in the 100 μm band. This again, might be because of the abundance of a certain kind of dust composition.

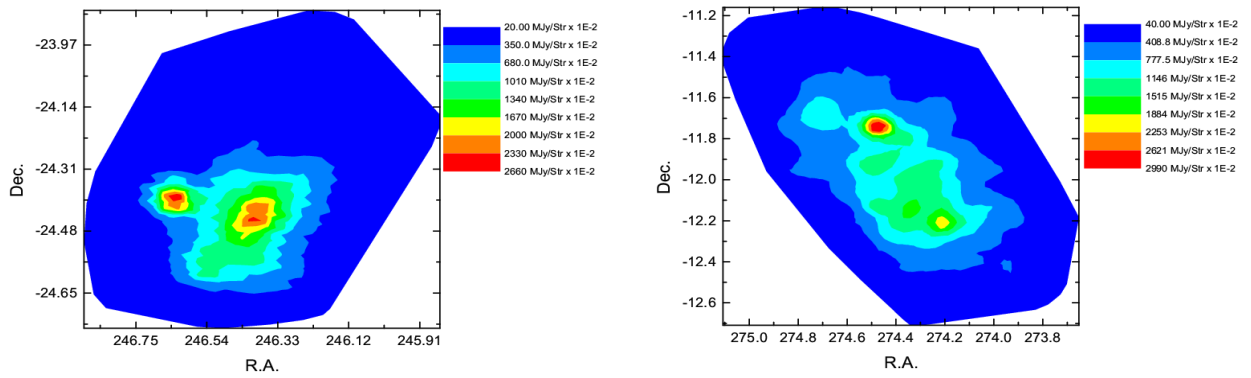

Fig. 5: *The distribution of 60μm flux density (background corrected) over Region-I (left) and Region-II (right).*

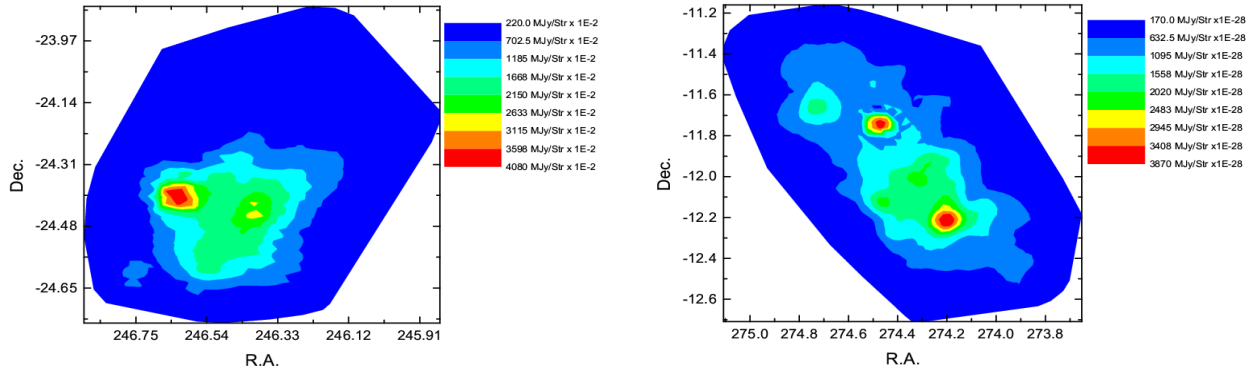

Fig. 6: *The distribution of 100 μm flux density (background corrected) over Region-I (left) and Region-II (right).*

Temperature Distribution

Using the method of Schnee *et al*. [13] we calculated dust color temperature of each pixel inside the outer contour of regions of interest. We used the IRAS 100 m and 60 m FITS images downloaded from the IRAS server. For the calculation of temperature we choose the value of $\beta = 2$ following the explanation given by Dupac *et al*.[9] The region with maximum and minimum temperature is found to lie in the range of 20.75 K to 35.90 K for Region-I and 22.52 K to 45.63 K for Region-II. The dust color temperature less than 20 K represents the interstellar cirrus cloud. Thus our far infrared dust structures are not cirrus clouds. The average temperature of the dust is 27.92 K for the first region and 31.61 K for the second region.

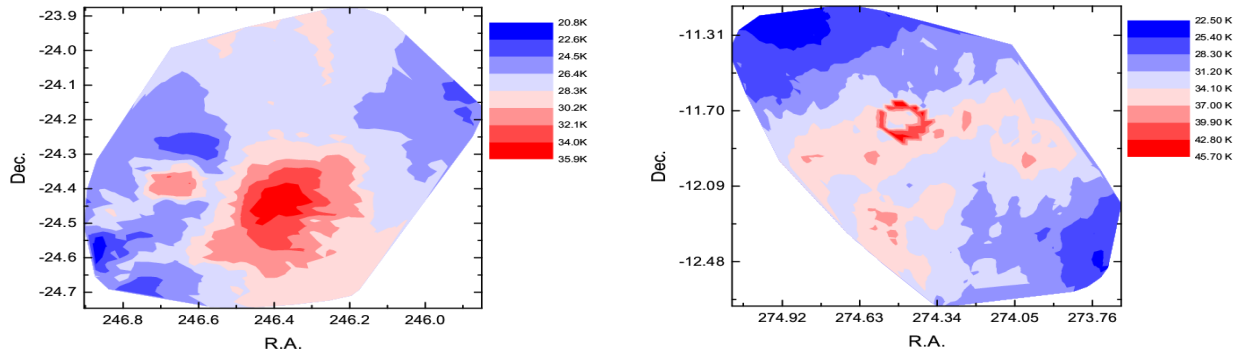

Fig. 7: *The distribution of dust temperature inside the outermost contours of the region of interests Region-I (left) and Region-II (right).*

For the first region, the temperature in this particular region is higher in the central part which then gradually decreases and reaches the minimum points in the edges. However, we can see that the distribution is not very uniform and fluctuates at some places. The maximum temperature in this region (Region-I) is found at R.A. (J2000) = 16h 25m 29.70s & Dec. (J2000) = 24˚27′ 06.8″ with a value of 35.71 K. While, the minimum temperature is found at R.A. (J2000) = 16h27m28.68s & Dec. (J2000) = 24˚34′58.8″ with a value of 20.75 K.

In the second region, however, we can see that temperature is higher in the upper central part and gradually decreases and reaches the minimum points in the edges. However, we can see that the distribution is fairly uniform with some fluctuations here and there. The maximum temperature in this region (Region-II) is found at R.A. (J2000) =18h17m58.91s& Dec. (J2000) =−11˚39′34.8″with a value of 35.71 K. While, the minimum temperature is found at R.A. (J2000) = 18h17m58.91s & Dec. (J2000) = 11˚39′34.8″ with a value of 45.63 K.

The following shows the maximum and minimum temperature zones in the regions of interest.

Table 1: The table shows the maximum dust color temperature within different contours in Region-I (353.01˚, 16.98˚).

Contour	**R.A. (J2000)**	**Dec.(J2000)**	**T_{max} (K)**
24 outer	$16^h25^m24.20^s$	−24˚24′00.1″	35.90
146 lower	$16^h26^m29.30^s$	−24˚24′00.1″	32.21
146 upper	$16^h25^m29.70^s$	−24˚27′06.8″	35.71

Table 2: The table shows the maximum dust color temperature within different contours in Region-II (18.42˚, 1.98˚).

Contour	**R.A. (J2000)**	**Dec.(J2000)**	**T_{max} (K)**
24 outer	$18^h16^m02.41^s$	−11˚57′33.8″	38.52
77 Big	$18^h17^m22.14^s$	−11˚50′04.8″	37.49
77 Small	$18^h18^m29.55^s$	−11˚42′34.5″	34.09
100 Big	$18^h17^m22.13^s$	−11˚09′34.8″	36.8
100 Medium	$18^h17^m58.91^s$	−11˚39′34.8″	45.63
100 Small	$18^h18^m47.92^s$	−11˚39′34.3″	31.58
131 Big	$18^h17^m09.85^s$	−11˚09′34.7″	34.67
131 Medium	$18^h17^m40.53^s$	−11˚45′34.8″	35.93
131 Small	$18^h17^m16.00^s$	−11˚03′34.7″	33.4

Table 3: The table shows the minimum dust color temperature within different contours in Region-I (353.01˚, 16.98˚).

Contour	**R.A. (J2000)**	**Dec.(J2000)**	**T_{max} (K)**
24 outer	$16^h27^m28.68^s$	−24˚34′58.8″	20.75
146 lower	$16^h26^m25.52^s$	−24˚26′19.7″	25.65
146 upper	$16^h25^m47.74^s$	−24˚24′44.2″	33.15

Table 4: The table shows the minimum dust color temperature within different contours in Region-II (18.42˚, 1.98˚).

Contour	R.A. (J2000)	Dec.(J2000)	T_{max} (K)
24 outer	$18^h16^m02.41^s$	−11˚14′03.5″	22.52
77 Big	$18^h17^m22.14^s$	−12˚15′34.0″	30.03
77 Small	$18^h18^m29.55^s$	−11˚36′34.1″	29.39
100 Big	$18^h17^m22.13^s$	−12˚14′04.3″	30.05
100 Medium	$18^h17^m58.91^s$	−11˚47′34.1″	40.67
100 Small	$18^h18^m47.92^s$	−11˚39′34.1″	30.57
131 Big	$18^h17^m09.85^s$	−12˚15′34.6″	28.99
131 Medium	$18^h17^m40.53^s$	−11˚47′04.7″	31.82
131 Small	$18^h17^m16.00^s$	−12˚00′34.8″	32.02

Mass Distribution

We used the method by Redman et. al [11] & Young et. al [12] to estimate the dust mass in our region of interest using 100 m IRAS image. The infrared flux is obtained from Groningen IRAS server available at official website of Sky View virtual observatory. By using the average of the maximum and minimum temperature of each maxima summing up of the flux density of each pixel inside the region, the value of average temperature and the total flux density for all the maxima can be known. For the calculation of the mass we need the distance to the region of interest. The distance 139 pc [5] is adopted for the first region and 2.6 kpc [8] is adopted for the second region. We used these distances in our calculation.

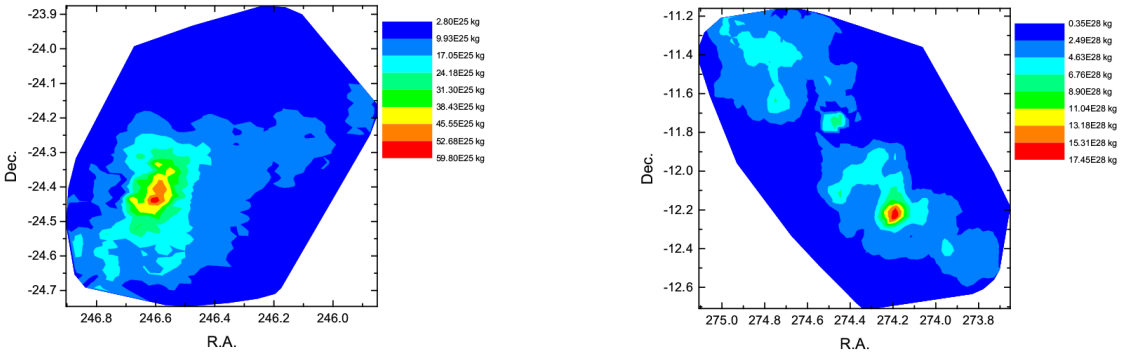

Fig. 8: *The distribution of dust mass inside the outermost contours of the region of interests Region-I (left) and Region-II (right).*

The distribution of the dust mass in Region-I seems to be fairly uniform with a maxima in the lower central part. The concentration of mass then gradually decreases and reaches minimum values around the edges. Here we can see that the dust mass of this structure is more or less concentrated towards a single point. This could mean that the dust cloud is in a phase of gravitational contraction around the maxima seen in the plot. However, the mass of dust in Region-II seems to be concentrated along the periphery of the major diameter. There seem to be two maxima in the region. One being in the upper half and the other in the lower half portion of the structure. However, the most amount of mass is concentrated in the lower half portion of the structure with a very sharp maxima. Also, in this region the dust clouds seem to clumped together into two separate dense structures suggesting gravitational contraction towards their respective maxima.

Comparison of Mass, Temperature and Flux along the Diameters

A comparison of the mass, temperature and flux along the diameters might be hinting towards an

interesting finding. What we see here in the diametric comparison of these quantities of the first region is that it the temperature and mass seem to be following along with the curve of flux density. Temperature and mass seem to rise and fall correspondingly with the flux density. However, just as the flux reaches maximum, the mass suddenly drops. Now, this could have some interesting reason for occurrence. We suspect that the average grain size around the maximum flux region is probably smaller than elsewhere. With a smaller size, and hence, a larger overall surface area, the smaller grains in the maximum flux area, could be responsible for the spike in flux, accompanying a decrease in the overall mass. This effect is not seen for the minor diameter, suggesting an even distribution of grain sizes. However, there is a slight drop in mass in the secondary maximum along the minor diameter, again directing towards a similar distribution of grain geometry.

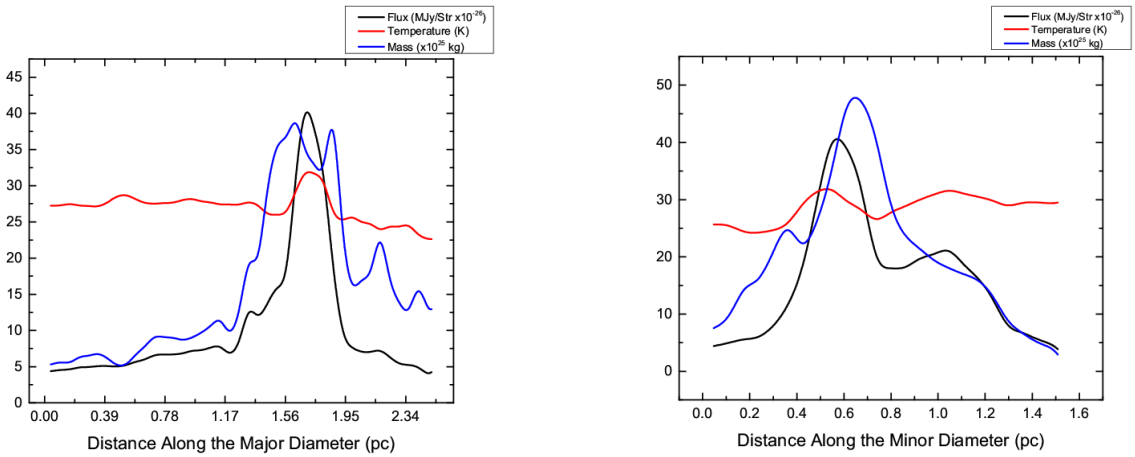

Fig. 9: *Comparison of the dust color temperature (red), mass (blue) and fluxdensity (black) of the dust cloud along the major diameter (left) and minor diameter (right) for Region-I.*

In the second region though, the temperature doesn't not seem to correlate well with the flux density. It even shows an opposite overall curvature compared to the flux in the minor diameter. Nevertheless, the mass distribution shows a suggestive correlation, although the slopes of mass curves compared flux density are significantly smaller than those in the first region. This somewhat suggests that the grain size decrease as we go deeper towards the maxima, both along the major and minor diameter, because of the gradual increase in slope of the flux density without a considerable rise in mass; which means smaller grains were required to account for the increasing flux, with a fairly constant mass distribution along the diameter.

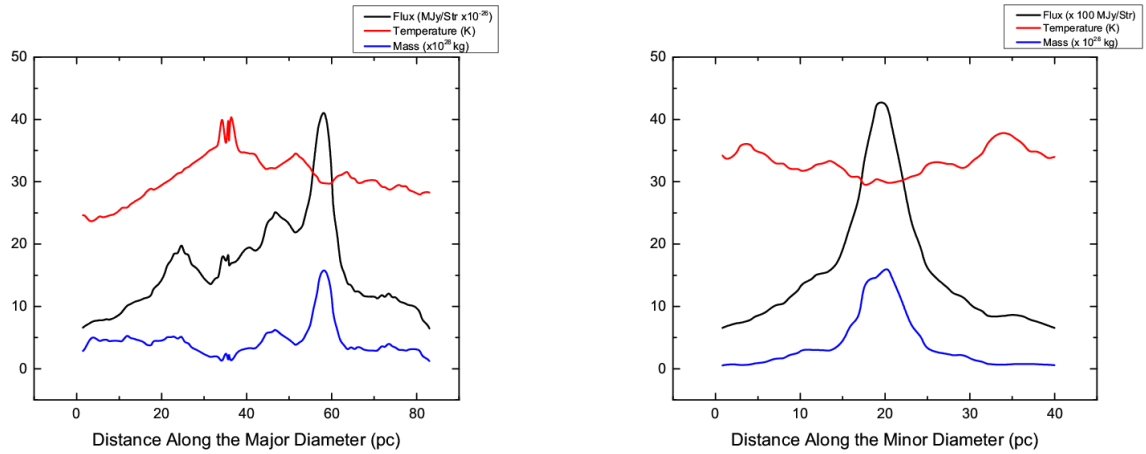

Fig. 10: *Comparison of the dust color temperature (red), mass (blue) and flux density (black) of the dust cloud along the major diameter (left) and minor diameter (right) for Region-II.*

Inclination Angles

Table 5: The inclination angles of different contour levels for varying intrinsic flatness (q*) for the first region, Region-I.

Intrinsic flatness (q*)	Inclination angle for Contour 24	Inclination angle for Contour 146 (Lower)	Inclination angle for Contour 146 (Upper)
0.13	53.91˚	57.01˚	24.69˚
0.15	54.17˚	57.3˚	24.78˚
0.17	54.47˚	57.63˚	24.88˚
0.19	54.81˚	58.01˚	24.99˚
0.21	55.18˚	58.44˚	25.11˚
0.23	55.61˚	58.92˚	25.25˚
0.25	56.08˚	59.45˚	25.4˚
0.27	58.71˚	61.99˚	30.82˚
0.29	59.65˚	63.01˚	31.76˚
0.31	60.71˚	64.15˚	32.77˚
0.33	54.06˚	57.09˚	25.68˚

Table 6: The inclination angles of different contour levels for varying intrinsic flatness (q*) for the first region, Region-II.

q*	24	77 (Large)	77 (Small)	100 (Large)	100 (Medium)	100 (Small)	131 (Large)	131 (Medium)	131 (Small)
0.13	71˚	67.18˚	30.57˚	64.41˚	32.78˚	32.44˚	42.63˚	37.38˚	50.32˚
0.15	71.55˚	67.63˚	30.68˚	64.81˚	32.9˚	32.56˚	42.8˚	37.52˚	50.55˚
0.17	72.2˚	68.16˚	30.81˚	65.26˚	33.04˚	32.7˚	43˚	37.69˚	50.81˚
0.19	72.96˚	68.76˚	30.95˚	65.79˚	33.2˚	32.85˚	43.23˚	37.87˚	51.11˚
0.21	73.85˚	69.45˚	31.11˚	66.38˚	33.37˚	33.02˚	43.48˚	38.08˚	51.44˚
0.23	74.89˚	70.25˚	31.29˚	67.06˚	33.56˚	33.21˚	43.75˚	38.31˚	51.81˚
0.25	76.12˚	71.16˚	31.48˚	67.83˚	33.78˚	33.42˚	44.06˚	38.56˚	52.21˚
0.27	79.31˚	73.81˚	35.95˚	70.35˚	37.96˚	37.65˚	47.31˚	42.25˚	54.99˚
0.29	81.87˚	75.43˚	36.82˚	71.7˚	38.82˚	38.51˚	48.14˚	43.09˚	55.88˚
0.31	86.29˚	77.42˚	37.77˚	73.28˚	39.75˚	39.44˚	49.06˚	44.00˚	56.87˚
0.33	70.73˚	67.03˚	31.31˚	64.33˚	33.45˚	33.12˚	43.03˚	37.91˚	50.55˚

Calculation of Jeans Mass

For the calculation of Jeans Mass of the structures, we used the equation,

$$M_J = C\left(\frac{kT}{m_H G}\right)^{3/2}\frac{1}{\rho^{1/2}} \dots\dots\dots\dots\dots\dots\dots\dots (7)$$

Here, we use C = 1, Boltzmann constant (k) = 1.38 × 10^{23} J K^{-1}, the average temperature of Region-I (T) = 27.92 K, and of Region-II (T) = 31.61 K, mean molecular weight of hydrogen gas (m_H) = 1.67 × 10^{-27} kg, Gravitational constant (G) = 6.67 × 10^{-11} N m^2 kg^{-2} and density of cloud is calculated by using the equation,

$$\rho = \left(\frac{3C}{4\pi}\right)^{2/3}\frac{kT}{m_H G R^2} \dots\dots\dots\dots\dots\dots\dots\dots (8)$$

Where, average radius of Region-I is R = 6.45 × 10^{16} m and that of Region-II is R = 1.89 × 10^{18} m.

For Region-I

From the equations 7 and 8, we get ρ= 2.73 × 10^{-22} kg m^{-3}. Jeans Mass (M_J) is found to be 3.6 × 10^{32} kg. Since, calculated mass of our structure is 4.17 × 10^{31} kg, which is much lesser than Jeans Mass. From this calculation of Jeans mass we conclude that our structure might not be star forming region.

For Region-II

For Region-II, we get ρ= 4.21 × 10^{-22} kg m^{-3}. Jeans Mass (M_J) is found to be 1.19 × 10^{34} kg. Since, calculated mass of our structure is 1.11 × 10^{34} kg, which is much lesser than Jeans Mass. From this calculation of Jeans mass we conclude that our structure might not be star forming region.

CONCLUSION

The diameter of the first nebular structure is found to be about ~ 2.61 pc × 1.57 pc, where major and minor diameters are 2.61 pc and 1.57 pc respectively. The diameter for the second nebular structure is found to be and ~82.99 pc × 39.99 pc, where major and minor diameters are and 82.99 pc and 39.99 pc. A study of flux density, temperature and mass variation along the diameters show a prominent condensation of dust and a Gaussian-like distribution is observed along major and minor diameters of the structure. Gaussian-like distribution suggests that the nebular structure is isolated and less disturbed from the external factors. A study of inclination angle suggests that the three-dimensional shape of the structures are not uniform and not regularly shaped.

The dust color temperature is found to lie in the range 20.75 K to 35.90 K for the first region and 22.52 K to 45.63 K for the second region. The total mass of dust in the first isolated structure is about 1.04 × 10^{29}kg (0.104 $M_\odot$) and the total mass of gas in the structure is found to be 4.17 × 10^{31} kg (20.99 $M_\odot$). Meanwhile, the total mass of dust in the second isolated structure is about 5.59 × 10^{31} kg (28.10 $M_\odot$) and the total mass of gas in the structure is found to be 1.11 × 10^{34} kg (5621.61$M_\odot$). The Jeans mass is found to be 3.59 × 10^{32} kg (180.99 $M_\odot$) for the first region and 1.19 × 10^{34} kg (6005.04 $M_\odot$) which is significantly greater than the total mass of the structure in both the cases, suggesting no star formation activity in the nebular structures of our interest.

ACKNOWLEDGEMENT

We are grateful to Prof. Dr. Binil Aryal for his valuable suggestions at many instances. We would like to thank St. Xavier's College faculty for their support; especially Dr. Binod Adhikari and Dr. Vinaya Kumar Jha for their inspiration to pursue this work. We would also like to thank Asst. Prof. Devendra Raj Upadhyaya for his suggestions during the data analysis phase.

REFERENCES

[1] Draine, B. T., & Li, A. Infrared emission from interstellar dust. IV. The silicate-graphite-PAH model in the post-Spitzer era. *The Astrophysical Journal*, *657*(2), 810 (2007).

[2] Mathis, J. S. Interstellar dust and extinction. *Annual Review of Astronomy and Astrophysics*, *28*(1), 37-70 (1990).

[3] Draine, B. T. Interstellar dust grains. *Annual Review of Astronomy and Astrophysics*, *41*(1), 241-289 (2003).

[4] Neugebauer, G., Habing, H. J., Van Duinen, R., Aumann, H. H., Baud, B., Beichman, C. A. & Emerson, J. P. The infrared astronomical satellite (IRAS) mission. *The Astrophysical Journal*, *278*, L1-L6 (1984).

[5] Mamajek, E. E. On the distance to the Ophiuchus star-forming region. *Astronomische Nachrichten*, *329*(1), 10-14 (2008).

[6] Allen, L. E., Myers, P. C., Di Francesco, J., Mathieu, R., Chen, H., & Young, E. Hubble Space Telescope/NICMOS Imaging Survey of the Ophiuchus (Lynds 1688) Cluster. *The Astrophysical Journal*, *566*(2), 993 (2002).

[7] Aryal, B., Paudel, S., &Saurer, W. Spatial orientations of galaxies in seven Abell clusters of BM type II. *Monthly Notices of the Royal Astronomical Society*, *379*(3), 1011-1021 (2007).

[8] Bica, E., Dutra, C. M., Soares, J., & Barbuy, B. New infrared star clusters in the Northern and Equatorial Milky Way with 2MASS. *Astronomy & Astrophysics*, *404*(1), 223-232 (2003).

[9] Dupac, X., Bernard, J. P., Boudet, N., Giard, M., Lamarre, J. M., Mény, C. & Torre, J. P. Inverse temperature dependence of the dust submillimeter spectral index. *Astronomy & Astrophysics*, *404*(1), L11-L15 (2003).

[10] Holmberg, E. *Medd. Lund. Ser.* II, No. 136 (1958).

[11] Redman, M. P., O'Connor, J. A., Holloway, A. J., Bryce, M., & Meaburn, J. A 500 km s^{-1} outflow from the young bipolar planetary nebula Mz 3. *Monthly Notices of the Royal Astronomical Society*, *312*(2) (2000).

[12] Young, K., Phillips, T. G., & Knapp, G. R. Circumstellar shells resolved in IRAS survey data. II-Analysis. *The Astrophysical Journal*, *409*, 725-738 (1993).

[13] Schnee, S. L., Ridge, N. A., Goodman, A. A., & Li, J. G. A complete look at the use of IRAS emission maps to estimate extinction and dust temperature. *The Astrophysical Journal*, *634*(1), 442 (2005).